Ultrasound in Med. & Biol., Vol. 35, No. 12, pp. 2055–2068, 2009

0301-5629/09/$–see front matter

ELSEVIER

doi:10.1016/j.ultrasmedbio.2009.08.003

● *Original Contribution*

USE OF NAKAGAMI STATISTICS AND EMPIRICAL MODE DECOMPOSITION FOR ULTRASOUND TISSUE CHARACTERIZATION BY A NONFOCUSED TRANSDUCER

Po-Hsiang Tsui,* Chien-Cheng Chang,*† Ming-Chih Ho,‡§ Yu-Hsin Lee,‡ Yung-Sheng Chen,¶ Chien-Chung Chang,# Norden E. Huang,*# Zhao-Hua Wu,** and King-Jen Chang‡§

*Division of Mechanics, Research Center for Applied Sciences, Academia Sinica, Taipei, Taiwan, ROC; †Institute of Applied Mechanics, National Taiwan University, Taipei, Taiwan, ROC; ‡Department of Surgery, National Taiwan University Hospital and College of Medicine, National Taiwan University, Taipei, Taiwan, ROC; §Angiogenesis Research Center, National Taiwan University, Taipei, Taiwan, ROC; ¶Department of Electrical Engineering, Yuan Ze University, Chung Li, Taiwan, ROC; #Research Center for Adaptive Data Analysis, National Central University, Chung Li, Taiwan, ROC; and **Department of Meteorology, Florida State University, Tallahassee, FL, USA

(*Received* 16 *December* 2008; *revised* 8 *July* 2009; *in final form* 5 *August* 2009)

Abstract—The Nakagami parameter associated with the Nakagami distribution estimated from ultrasonic backscattered signals reflects the scatterer concentration in a tissue. A nonfocused transducer does not allow tissue characterization based on the Nakagami parameter. This paper proposes a new method called the noise-assisted Nakagami parameter based on empirical mode decomposition of noisy backscattered echoes to allow quantification of the scatterer concentration based on data obtained using a nonfocused transducer. To explore the practical feasibility of the proposed method, the current study performed experiments on phantoms and measurements on rat livers *in vitro* with and without fibrosis induction. The results show that using a nonfocused transducer makes it possible to use the noise-assisted Nakagami parameter to classify phantoms with different scatterer concentrations and different stages of liver fibrosis in rats more accurately than when using techniques based on the echo intensity and the conventional Nakagami parameter. However, the conventional Nakagami parameter and the noise-assisted Nakagami parameter have different meanings: the former represents the statistics of signals backscattered from unresolvable scatterers, whereas the latter is associated with stronger resolvable scatterers or local inhomogeneity caused by scatterer aggregation. (E-mail: mechang@gate.sinica.edu.tw; mcho1215@ntu.edu.tw) © **2009 World Federation for Ultrasound in Medicine & Biology.**

Key Words: **Nakagami distribution, Empirical mode decomposition, Tissue characterization.**

INTRODUCTION

Ultrasonic backscattered echoes may be treated as random signals. The probability density function (pdf) of backscattered echoes can be modeled using appropriate statistical distributions to characterize the related tissue. In mathematics, a pdf is a function that represents a probability distribution using integrals. A Rayleigh distribution was the first model used to describe the statistics of backscattered signals (Burckhardt 1978), where the pdf of the backscattered envelope conforms to the Rayleigh distribution when the resolution cell of the transducer—which is a volume of space that is determined by the pulse length and the horizontal and vertical beam widths of the transmitted ultrasound—contains a large number of randomly distributed scatterers. The scatterers in most biological tissues have various possible arrangements, which has led to the application of distributions such as the Rician (Wagner et al. 1987), K (Weng et al. 1991), homodyned K (Dutt and Greenleaf 1994) and generalized K (Shankar 1995) to encompass non-Rayleigh statistics of the backscattered envelope, classified into pre-Rayleigh, Rayleigh and post-Rayleigh distributions (Wagner et al. 1987; Shankar 2000).

The Nakagami distribution initially proposed to describe radar echo statistics has subsequently been applied to model the statistics of ultrasonic backscattering (Hampshire et al. 1988; Zimmer et al. 1996; Shankar 2000; Wachowiak et al. 2002). It is a general model for all scattering conditions encountered in medical

Address correspondence to: Chien-Cheng Chang, Ming-Chih Ho. E-mail: mechang@gate.sinica.edu.tw (C.-C.C.), mcho1215@ntu.edu.tw (M.-C.H.)

ultrasound, including pre-Rayleigh, Rayleigh and post-Rayleigh distributions. The Nakagami parameter of the Nakagami distribution is particularly useful for differentiating different scatterer concentrations in a medium (Shankar 2000; Tsui and Wang 2004), and has been used to quantify scatterer properties in real tissues, including bone (Wang and Tsai 2001; Wang and Tsui 2004), skin (Raju and Srinivasan 2002), breast (Shankar et al. 2001, 2003) and blood (Cloutier et al. 2004; Huang and Wang 2007). There have been subsequent developments in the Nakagami model in two areas: (1) compounding Nakagami models to improve the fit with envelope statistics (Shankar 2003, 2004; Karmeshu and Agrawal 2006; Nadarajah 2007) and (2) the use of Nakagami-based imaging techniques to visually characterize tissues (Tsui and Chang 2007; Tsui et al. 2007, 2008a, 2008b).

Estimating the Nakagami parameter is notably affected by the focusing of the ultrasonic transducer. Using a focused transducer is useful for identifying different scatterer concentrations (Tsui and Wang 2004) because the focused transducer has a small resolution cell, making the statistics of backscattered signals vary with the scatterer concentration. Contrarily, a large resolution cell of the nonfocused transducer makes the numbers of scatterers in the resolution cell for various scatterer concentrations larger than 10, which leads to a nearly Rayleigh distribution for the statistics of different scatterer concentrations (Oosterveld et al. 1985; Tuthill et al. 1988; Zagzebski et al. 1999).

Using a focused transducer to estimate the statistical parameter also has drawbacks. First, the backscattered echoes measured by a focused transducer can be degraded by transducer focusing and beam diffraction, which increases the downshift of the ultrasonic signals in the central frequency region (Bevan and Sherar 2001) and produces weak and noisy echoes in the far field of the transducer. These factors not only affect statistical parameter estimation but also limit the datalength acquired for analysis. Second, to better understand the scattering properties of the medium, we may need to simultaneously calculate the backscattering coefficient for analyzing the backscattering cross section of scatterers (Shung and Thieme 1993). However, using a focused transducer could produce errors (Yuan and Shung 1986, Wang and Shung 1997), and hence an unfocused transducer might be better than a nonfocused one for increasing the spatial extent of the analysis and allowing the correct calculation of the backscattering coefficient.

Recent findings show that the statistics of backscattered signals measured by a nonfocused transducer vary with the scatterer concentration after applying an adaptive threshold filter to process ultrasonic radiofrequency (RF) signals. The adaptive threshold filter developed by Tsui et al. (2008c) is based on noise-assisted empirical mode decomposition (EMD) (Huang et al. 1998), which is the key part of the Hilbert-Huang transform (HHT) (Huang et al. 1998, 1999). Its performance is the same as that of the conventional thresholding technique based on applying a cutoff value for rejecting small echoes, but different in that it does not change the waveform features of the preserved signals. Based on this point, the backscattered RF echoes after adaptive threshold filtering may be used to calculate the Nakagami parameter for quantifying the corresponding statistical distribution and the scatterer properties. We call this method the noise-assisted Nakagami parameter, which endows a nonfocused transducer with the ability to characterize scatterers.

This paper describes phantom experiments carried out to explore the practical feasibility of the method based on the noise-assisted Nakagami parameter. In particular, the current work involved performing measurements on rat livers *in vitro* to evaluate the performance of the proposed method in practice. The next section introduces the theoretical background (including EMD), the adaptive threshold filter and defines the noise-assisted Nakagami parameter. Subsequent sections describe the experimental materials and methods and present the results along with a discussion of the meanings, advantages, and limitations of the noise-assisted Nakagami parameter. The final section provides concluding remarks.

THEORETICAL BACKGROUND

Empirical mode decomposition

EMD is the key component of the HHT proposed as an adaptive time–frequency analysis method for nonlinear and nonstationary data (Huang et al. 1998, 1999). EMD was developed with the aim of meaningfully determining the instantaneous frequency of a signal. Mathematically, the instantaneous frequency of a signal may be defined using the Hilbert transform. The Hilbert transform $Y(t)$ of an arbitrary time series $X(t)$ is given by

$$Y(t) = \frac{1}{\pi} P \int_{-\infty}^{\infty} \frac{X(t')}{t-t'} dt'. \quad (1)$$

With this definition, $X(t)$ and $Y(t)$ form a complex conjugate pair, and therefore the analytic signal $Z(t)$ can be defined as

$$Z(t) = X(t) + iY(t) = a(t)e^{i\theta(t)}, \quad (2)$$

where

$$a(t) = \left[X^2(t) + Y^2(t)\right]^{1/2} \quad (3)$$

and

$$\theta(t) = \arctan\left(\frac{Y(t)}{X(t)}\right) \quad (4)$$

The instantaneous frequency can then be defined as

$$\omega(t)=\frac{d\theta(t)}{dt}. \tag{5}$$

The definition in eqn (5) places some restrictions on the input data. First, the instantaneous frequency has a single value at any given time, and hence can only describe monocomponent data. Because there is no precise definition of a monocomponent, researches have considered only narrowband data to ensure that the instantaneous frequency makes sense (Schwartz et al. 1966). Second, for any function to have a meaningful instantaneous frequency, the real part of its Fourier transform should only consist of positive frequency components (Boashash 1992). Note that this constitutes a global restriction of the Fourier transform. There are some crucial restrictions of Fourier spectral analysis: the system must be linear, and the data must be strictly periodic or stationary; otherwise, the resulting spectrum will make little physical sense (Huang et al. 1998). This restriction may not be useful for nonstationary data, and most physical-world data are nonstationary. To determine the instantaneous frequency of nonstationary data, it is necessary to develop a modified version of the restriction that can be applied locally (Huang et al. 1998).

To satisfy the previous restrictions, Huang et al. (1998) defined a class of functions called intrinsic mode functions (IMFs) that allow the instantaneous frequency to be defined at any given time point. Actually, the IMF is a single-component signal that fulfills the following conditions: (1) the number of zero and extreme crossings does not exceed one in the entire dataset, and (2) the mean value of the up and down envelopes, which are defined using local maxima and minima, respectively, is zero at any time (this means that two envelope curves are symmetrical relative to the time axis). Huang et al. (1998) further developed the EMD method to decompose a signal into a set of IMFs for calculating their instantaneous frequencies using the Hilbert transform. This is the so-called HHT; that is, the Hilbert transform of IMFs obtained by EMD for time–frequency analysis. The EMD algorithm is explained next.

We first find the local maxima and minima of signal $x(t)$ and use cubic spline interpolation to obtain its up and down envelopes. If the mean of these two envelopes is $d_1(t)$, the difference between the signal and $d_1(t)$ is the first component,$h_1(t)$:

$$h_1(t) = x(t)-d_1(t). \tag{6}$$

This is called the sifting process. We have to judge whether $h_1(t)$ is an IMF. Ideally, if the cubic spline interpolation is perfect and there is no gentle hump on the signal slope, $h_1(t)$ should satisfy all IMF requirements. However, in reality, imperfect fitting commonly produces overshoots and undershoots that generate new extrema and shift or exaggerate the existing ones. Even if the fitting is perfect, humps may become local extrema after the first round of sifting. The envelope mean may also differ from the true local mean of the signal for nonstationary data, resulting in an asymmetric waveform. Therefore, the sifting process has to be repeated k times until $h_{1k}(t)$ is an IMF. $h_1(t)$ is treated as the original data in the second sifting process:

$$h_1(t)-d_{11}(t) = h_{11}(t). \tag{7}$$

The sifting process is repeated k times until we find $h_{1k}(t)$, which is an IMF:

$$h_{1(k-1)}(t)-d_{1k}(t) = h_{1k}(t). \tag{8}$$

Then we define

$$c_1(t) = h_{1k}(t) \tag{9}$$

as the first IMF component (*i.e.*, component C1) for the data. Here we used the stopping criterion for the sifting process proposed by Huang et al. (1998). This is accomplished by limiting the standard deviation (SD) computed from the two consecutive sifting results as

$$SD = \sum_{t=1}^{T}\left[\frac{|h_{1(k-1)}(t)-h_{1k}(t)|^2}{h_{1(k-1)}(t)}\right] \tag{10}$$

The SD is typically set between 0.2 and 0.3. Overall, C1 contains the finest and the shortest period component of the signal. Subsequently, we can subtract $c_1(t)$ from the signal:

$$x(t)-c_1(t) = S_1(t). \tag{11}$$

Because residue $S_1(t)$ still contains information about components with longer periods, we treat it as the new original data and apply the same sifting process as described before. This procedure can be repeated for all subsequent $S_j(t)$ values, yielding

$$S_1(t)-c_2(t) = S_2(t), \ \ldots, \ S_{n-1}(t)-c_n(t) = S_n(t). \tag{12}$$

Summing eqns (11) and (12) finally yields

$$x(t) = \sum_{i=1}^{n} c_i(t)+S_n(t). \tag{13}$$

This indicates that $x(t)$ is decomposed by EMD into n IMFs and a residue $S_n(t)$, which is the signal trend with, at most, one extremum or a constant.

Adaptive threshold filter

Compared with the conventional threshold technique based on a specific threshold value, the adaptive threshold

filter based on the noise-assisted EMD was proposed to suppress the small echoes without any waveform deformation of the preserved significant echoes (Tsui et al. 2008c). The algorithm is illustrated in Fig. 1 and summarized as: (i) add artificial white noise to the ultrasonic RF signals, (ii) apply EMD to the noisy backscattered RF data, and (iii) take the C1 IMF component as the filtered output. We explain the basis of the algorithm as follows. White noise has a wide bandwidth (ideally an infinite bandwidth) and hence is likely to contain fluctuations at higher frequencies than those in the ultrasonic signal, producing additional local extrema in the waveform of the received backscattered RF signal. Adding an appropriate level of white noise to the backscattered RF data will mean that the echoes themselves contribute to local extrema for larger echoes, whereas those for small echoes come from noise-induced fluctuations. Under this condition, the C1 component obtained from EMD of the noisy backscattered RF signals shows larger echoes, whereas the part corresponding to small signals is replaced by a noise-scale baseline. The performance of the adaptive threshold filter is fully described elsewhere (Tsui et al. 2008c).

Figure 2a shows a B-mode image of the carotid artery. Figure 2b shows one scan line of the backscattered signals corresponding to the position indicated by the white dotted line in Fig. 2a. Small echoes between the upper and lower vessel walls contaminate the image, making it difficult to see fine details of these walls. To remove the small signals, we added white noise at different levels so as to adjust the SNR from 25–15 dB and then applied EMD to the noisy RF data to obtain the filtered results, as shown in Fig. 2c–2e. It is evident from this figure that decreasing the SNR (*i.e.*, adding more noise) gradually reduces the small signals associated with echoes between the vessel walls. The figure also shows that the adaptive threshold filter does not deform any of the important waveform features, thereby preserving large echoes. In contrast, the waveform characteristics are destroyed by applying a conventional single threshold, as shown in Fig. 2f.

Noise-assisted Nakagami parameter

The pdf of backscattered envelope R under the Nakagami statistical model is given by

$$f(r) = \frac{2m^m r^{2m-1}}{\Gamma(m)\Omega^m}\exp\left(-\frac{m}{\Omega}r^2\right)U(r), \qquad (14)$$

where $\Gamma(.)$ and $U(.)$ are the gamma function and the unit step function, respectively. Let $E(.)$ denote the statistical mean; then scaling parameter Ω and Nakagami parameter m associated with the Nakagami distribution can be respectively obtained from

$$\Omega = E\left(R^2\right) \qquad (15)$$

and

$$m = \frac{\left[E(R^2)\right]^2}{E\left[R^2 - E(R^2)\right]^2}. \qquad (16)$$

Nakagami parameter m represents a shape parameter determined by the pdf of the backscattered envelope. As m varies from 0 to 1, the envelope statistics change from a pre-Rayleigh to a Rayleigh distribution, and the statistics of the backscattered signal conform to post-Rayleigh distributions if m is larger than 1, as shown in Fig. 3.

Note that using eqn (16) to estimate the Nakagami parameter has a prerequisite: the ultrasonic data used must conform to the Nakagami distribution. This prerequisite ensures that the Nakagami parameter estimated from ultrasonic data describes the statistical distribution of the envelope signal. Previous studies have shown that both the raw backscattered signals and the bandpass-filtered echoes conform to the Nakagami distribution (Shankar 2000; Dumane and Shankar 2001). Considering that the EMD is a process of bandpass filtering (Flandrin et al. 2004), the IMFs are essentially the bandpass data of backscattered echoes, representing that the IMFs conform to the Nakagami distribution. Moreover, it has been shown that the adaptive threshold filter based on EMD does not change the important waveform features of the preserved backscattered echoes (Tsui et al.

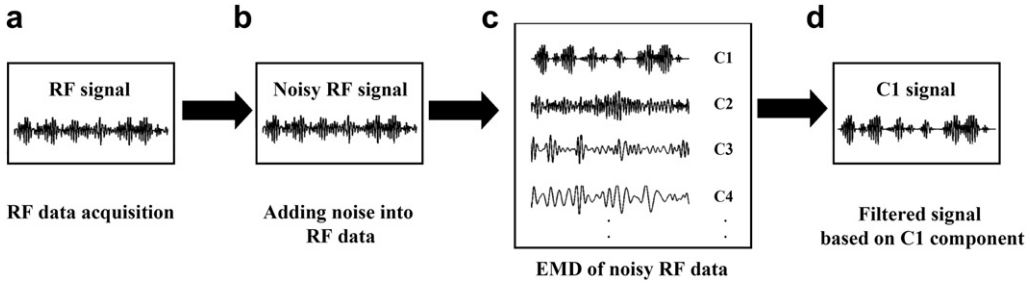

Fig. 1. Flow chart for the algorithm of the adaptive threshold filter: (a) an RF signal; (b) the noisy RF signal obtained by adding white noise to the signal in (a); (c) EMD of the noisy RF signal; and (d) taking component C1 as the filtered signal. Refer to eqn (9) for the meaning of component C1.

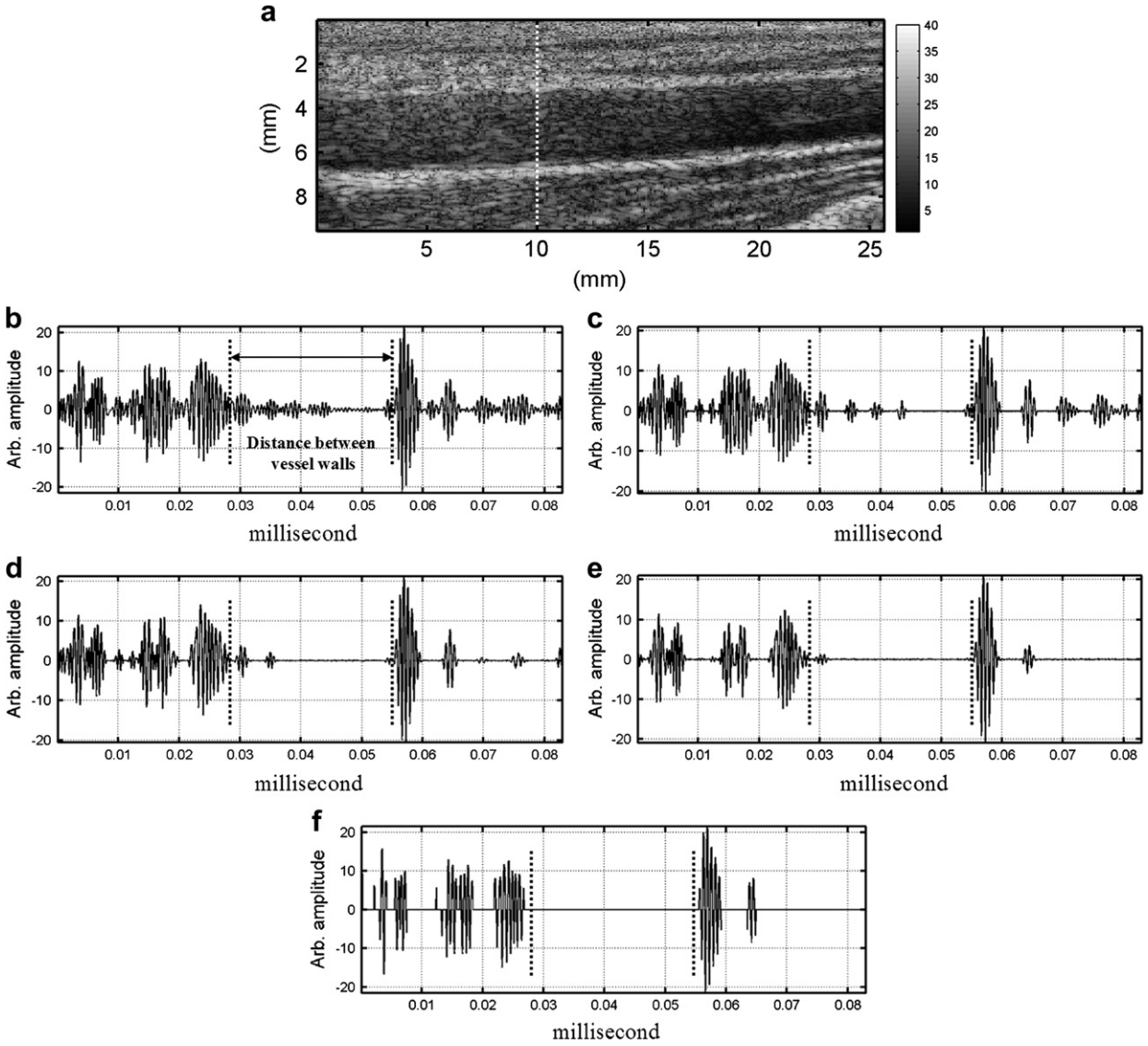

Fig. 2. An example of adaptive threshold filtering: (a) B-mode image of the carotid artery; (b) a typical backscattered RF signal corresponding to the position indicated by the white dotted line in the carotid B-mode image; (c–e) the backscattered RF signals after adaptive threshold filtering by adjusting the SNR to be 25, 20 and 15 dB, respectively; and (f) the RF signal after the conventional thresholding process (threshold value=5).

2008c). These factors indicate that the statistics of the backscattered RF echoes can be quantified directly after adaptive threshold filtering by estimating the so-called noise-assisted Nakagami parameter as

$$m_{\mathrm{C1}} = \frac{[E(R_{\mathrm{C1}})]^2}{E[R_{\mathrm{C1}} - E(R_{\mathrm{C1}})]^2}, \tag{17}$$

where R_{C1} represents the envelope of the ultrasonic signal after adaptive threshold filtering (*i.e.*, the C1 component signal obtained from EMD of the noisy RF signals). The next section describes phantom experiments and liver measurements obtained *in vitro* aimed at determining the practical feasibility of the proposed method.

EXPERIMENTS

Phantom experiments

The phantoms mimicking soft tissues with different concentrations of scatterers were made by adding different weights of glass beads (Model 59200U, Supelco, Bellefonte, PA, USA) with an average diameter of 75 μm into agar produced by dissolving 0.75 g of agar powder in 100 mL of water. The scatterer concentration (SC; in units of number of scatterers per cubic millimeter) in the phantom was

$$\mathrm{SC} = \frac{M}{\frac{4}{3}\pi \ r_{\mathrm{g}} \bullet \rho \bullet V}, \tag{18}$$

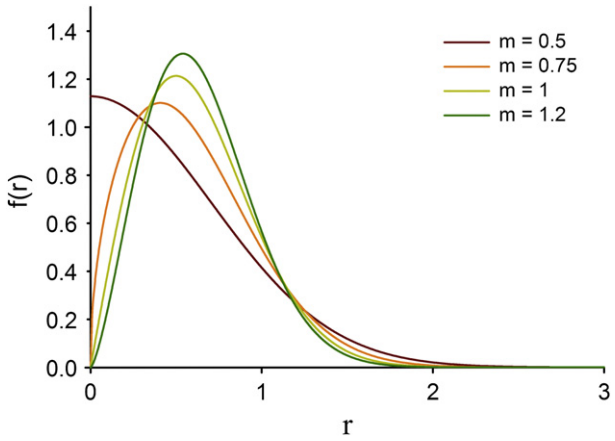

Fig. 3. Nakagami distributions for different values of the Nakagami parameter (Reproduced with permission from IOP Publishing, Tsui et al., 2008b).

where M, r_g and ρ correspond to the mass, radius and density of the glass beads, and V denotes the volume of the agar phantom. We produced phantoms with scatterer concentrations of 2, 4, 8, 16 and 32 scatterers/mm^3 for experimental measurements.

A single-crystal ultrasound imaging system was constructed for scanning the phantom to acquire the ultrasonic backscattered signals associated with different scatterer concentrations. The system comprised a mechanical scanning assembly, a single-element transducer, a pulser/receiver and a data acquisition card, as shown in Fig. 4 and explained later. The transducer was mechanically scanned using a high-resolution motion stage driven by a piezoelectric motor (Model HR8, Nanomotion, Yokneam, Israel). Using a piezoelectric motor reduced the noise level, which improved the quality of received ultrasonic echoes. The transducer was driven by a pulser/receiver (Model 5072PR, Panametrics-NDT, Waltham, MA, USA) for transmitting and receiving ultrasonic signals. The received RF echoes backscattered from the phantom were amplified with the built-in 59-dB amplifier in the pulse/receiver and then digitized by an analog-to-digital converter (Model PXI-5152, National Instruments, Austin, TX, USA) for data storage and offline analysis in a personal computer.

A 5-MHz cylindrically nonfocused transducer with a diameter of 13 mm was used (Model A309R, Panametrics-NDT). Before the experiments, the acoustic characteristics of the transducer were measured using a hydrophone (Model HNP-0400, ONDA, Sunnyvale, CA) mounted on a positioner controlled by a 3-D stepping motor. The natural focal length was 14 cm. The –3 dB beamwidth and pulse length at the natural focal zone were 3.6 mm and 0.85 mm, respectively. On the other hand, the pulse-echo substitution method was used to measure attenuation coefficients of the phantoms. The attenuation coefficients for the scatterer concentrations of 2, 4, 8, 16 and 32 scatterers/mm^3 were 0.012, 0.019, 0.025, 0.037 and 0.069 nepers/cm at 5 MHz, respectively. We then placed the transducer and a phantom on the holder in a bath containing distilled water at a temperature of about 25 °C. The distance between the transducer and the phantom was 2 cm, corresponding to the near field. For each phantom, we acquired 50 A-lines of backscattered RF signals at a sampling rate of 50 MHz. Each backscattered signal corresponded to a spatial-analysis length of about 7 mm. The noise-assisted Nakagami parameter was accurately estimated using attenuation coefficients of the phantoms to correct for signal attenuation. In principle, the noise-assisted Nakagami parameter may be smaller before attenuation correction than after attenuation correction because the decrease in the signal amplitude tends to make the statistics of the extracted backscattered signals based on the C1 signal closer to a pre-Rayleigh distribution. Subsequently, we added artificial white noise to the backscattered RF echoes to adjust the SNR from 40–25 dB using the ''awgn'' (add white Gaussian noise to a signal) function in MATLAB software (The MathWorks, Natick, MA, USA). The envelopes of the noisy backscattered RF signals were used to calculate the relative echo intensity and the noise-assisted Nakagami parameter as functions of scatterer concentration. The relative echo intensity was calculated based on the scaling parameter of the Nakagami distribution described by eqn (15).

Tissue measurements in vitro

Four male 7-week-old Wistar rats weighing between 210 and 230 g were used. The Institutional Animal Care and Use Committee in Taiwan University Hospital approved the use of the rats in this study. The rats were bred and maintained in an air-conditioned animal house with food and water. Liver fibrosis was induced in each rat by an intraperitoneal injection of 0.5% dimethylnitrosamine (DMN) at 2mL/kg of body weight for three consecutive days each week (George et al. 2001). To induce different degrees of liver fibrosis in the rats, DMN injections were applied to the rats for different numbers of weeks, as illustrated in Fig. 5: rat 1 was the normal case, and rats 2, 3 and 4 received DMN injections for 3, 5 and 6 weeks, respectively. Each rat was sacrificed after a rest period of 2 weeks and the liver was excised. Ultrasound scanning was applied to the left lateral lobe of the liver. The left lobe had a thickness between 1 and 1.5 cm, and a length and width of between 2 and 4 cm. The experimental setup and procedure used to measure liver specimens was the same as that for the phantom experiments. For each liver specimen, 50 A-lines of backscattered signals were acquired from the same 5-MHz nonfocused transducer using the same system at a sampling rate of 50 MHz. Each backscattered signal also corresponded to a spatial-analysis length of 7 mm. Five independent

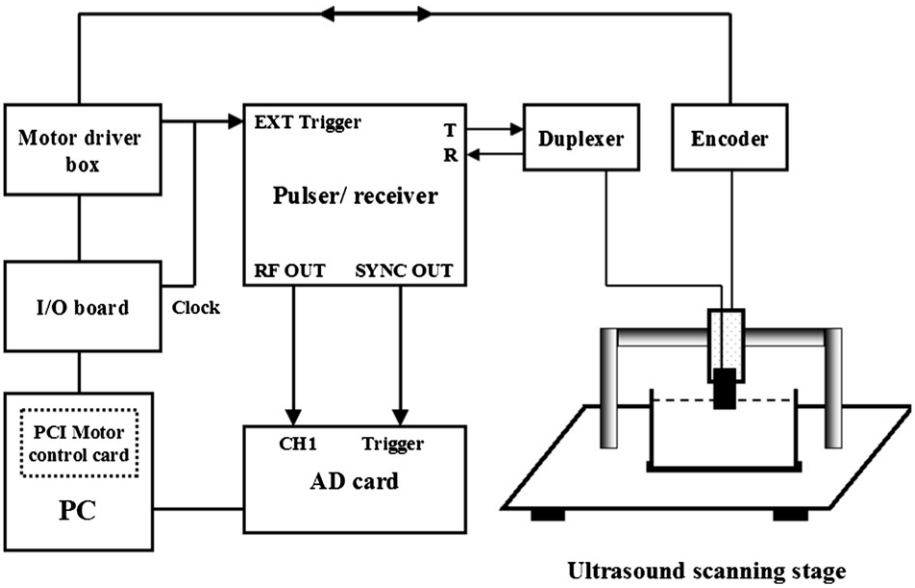

Fig. 4. Imaging system setup for measurements on phantoms and liver specimens.

measurements were made to allow calculation of the mean and SD values of the echo intensity, Nakagami parameter m and noise-assisted Nakagami parameter m_{C1}.

The attenuation correction was ignored in the measurements of liver fibrosis *in vitro* because different stages of liver fibrosis may exhibit different attenuations, which implies that backscattered signals with different attenuations need different SNR adjustments for estimating the noise-assisted Nakagami parameter. This may be overcome by choosing the appropriate SNR for specimens with different attenuations based on knowledge of the relationship between the attenuation coefficient and the SNR. Nevertheless, such guidance may be difficult to follow *in vivo* and in clinical conditions, because real tissues with complex structural compositions increase the difficulty of estimating attenuation information. Consequently, this investigation purposely did not compensate for attenuation in the liver measurements to evaluate whether the attenuation effect markedly affects the performance of the noise-assisted Nakagami parameter.

To score the level of liver fibrosis for each rat, the liver specimen was fixed in 10% neutral-buffered formalin, embedded in paraffin, and sliced into 4-μm-thick sections for histological analysis with the hematoxylin and eosin (H&E) staining method. The tissue sections for histological examinations were 10–15 mm in diameter. The insonified regions did not necessarily correspond to those examined histologically. To avoid sampling errors, we prepared five histological sections from different areas for each liver specimen. The Metavir score, which quantifies the degree of liver fibrosis, was determined by an experienced pathologist who was blinded to the treatment protocol. The pathologist identified homogenously distributed fibrosis induced throughout the liver parenchyma, and the extent of liver fibrosis was found to be proportional to the duration of the DMN injection.

RESULTS AND DISCUSSION

Phantom experiments

Figure 6a shows the ultrasonic backscattered signals after adaptive threshold filtering (the C1 component signal from EMD of the noisy backscattered RF data) for scatterer concentrations ranging from 2–16 scatterers/mm^3

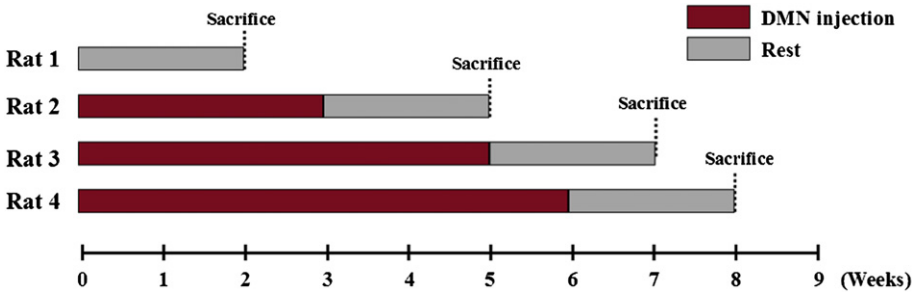

Fig. 5. Schedule of DMN injections for each rat.

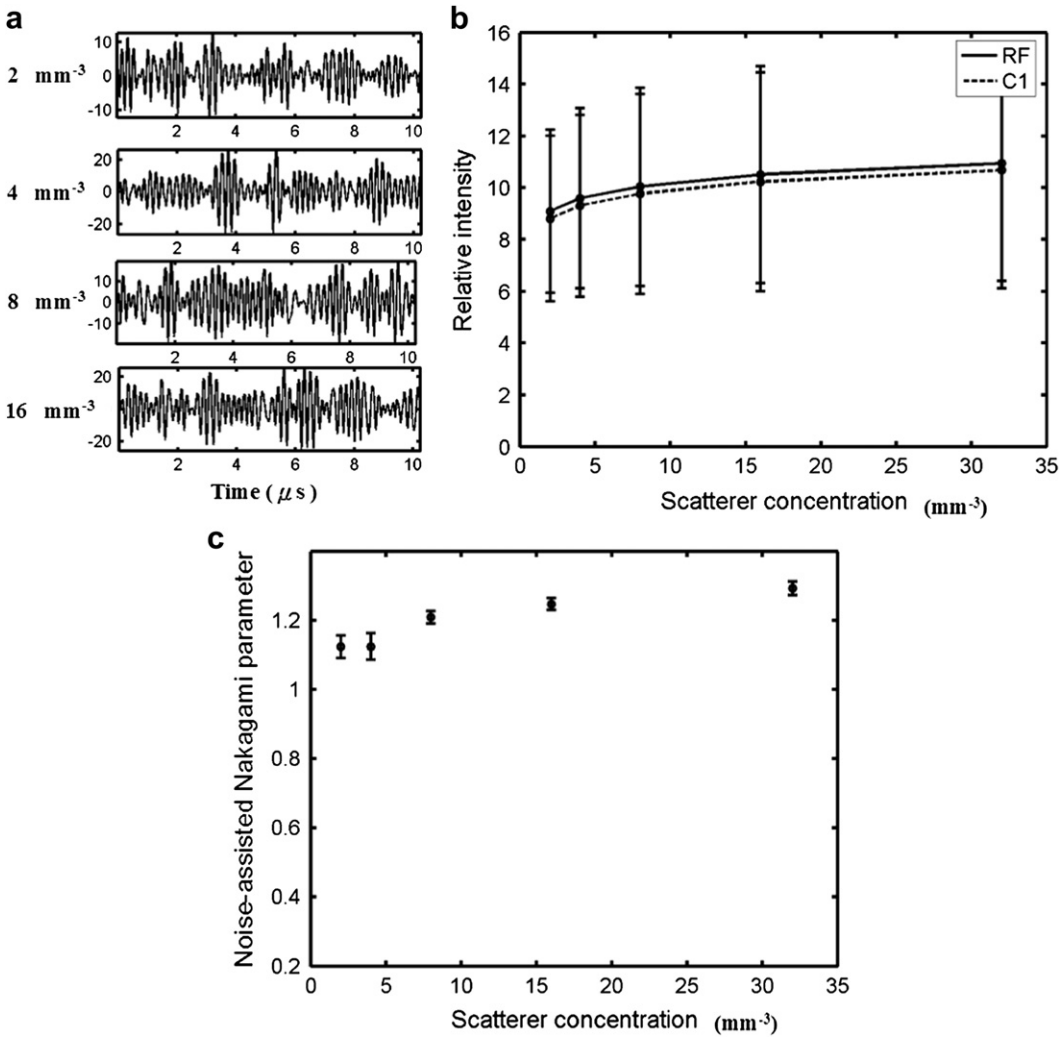

Fig. 6. (a) Filtered signals (component C1) for scatterer concentrations from 2–16 scatterers/mm^3 (from top to bottom); (b) the relative echo intensity as a function of scatterer concentration for backscattered RF data and the C1 signal; and (c) the noise-assisted Nakagami parameter as a function of scatterer concentration. The SNR for adaptive threshold filtering was 40 dB.

when the SNR was adjusted to 40 dB. Figure 6b and 6c show the relative echo intensity and the noise-assisted Nakagami parameter as functions of scatterer concentrations ranging from 2–32 scatterers/mm^3, respectively. The echo intensity of the backscattered RF data increased from about 9–11 as the scatterer concentration increased because of a larger number of scatterers producing a stronger backscattering signal. On the other hand, the noise-assisted Nakagami parameter varied between 1.1 and 1.25 over the same range of scatterer concentrations. This trend is similar to the previous result for the Nakagami parameter as a function of scatterer concentration measured by a nonfocused transducer (Tsui and Wang 2004). That study used raw backscattered echoes to estimate the Nakagami parameter, whereas the present study used C1-based backscattered signals to estimate the noise-assisted Nakagami parameter. Thus, the Nakagami and noise-assisted Nakagami parameters may have different physical meanings. The reason why the Nakagami parameter is close to the noise-assisted Nakagami parameter is that artificial noise exerts only a small effect on the RF signals for an SNR of 40 dB. Therefore, the C1-based backscattered signals after adaptive threshold filtering are approximately equivalent to the original backscattered RF echoes before filtering, approximately corresponding to a Rayleigh distribution for different scatterer concentrations. This is also the reason why the echo intensity as a function of scatterer concentration for the C1 signal agrees well with that for the original ultrasonic RF data (Fig. 6b).

Figure 7a shows the C1-based backscattered signals after adaptive threshold filtering for scatterer concentrations ranging from 2–16 scatterers/mm^3 when the SNR was adjusted to 30 dB (*i.e.*, with the artificial noise having

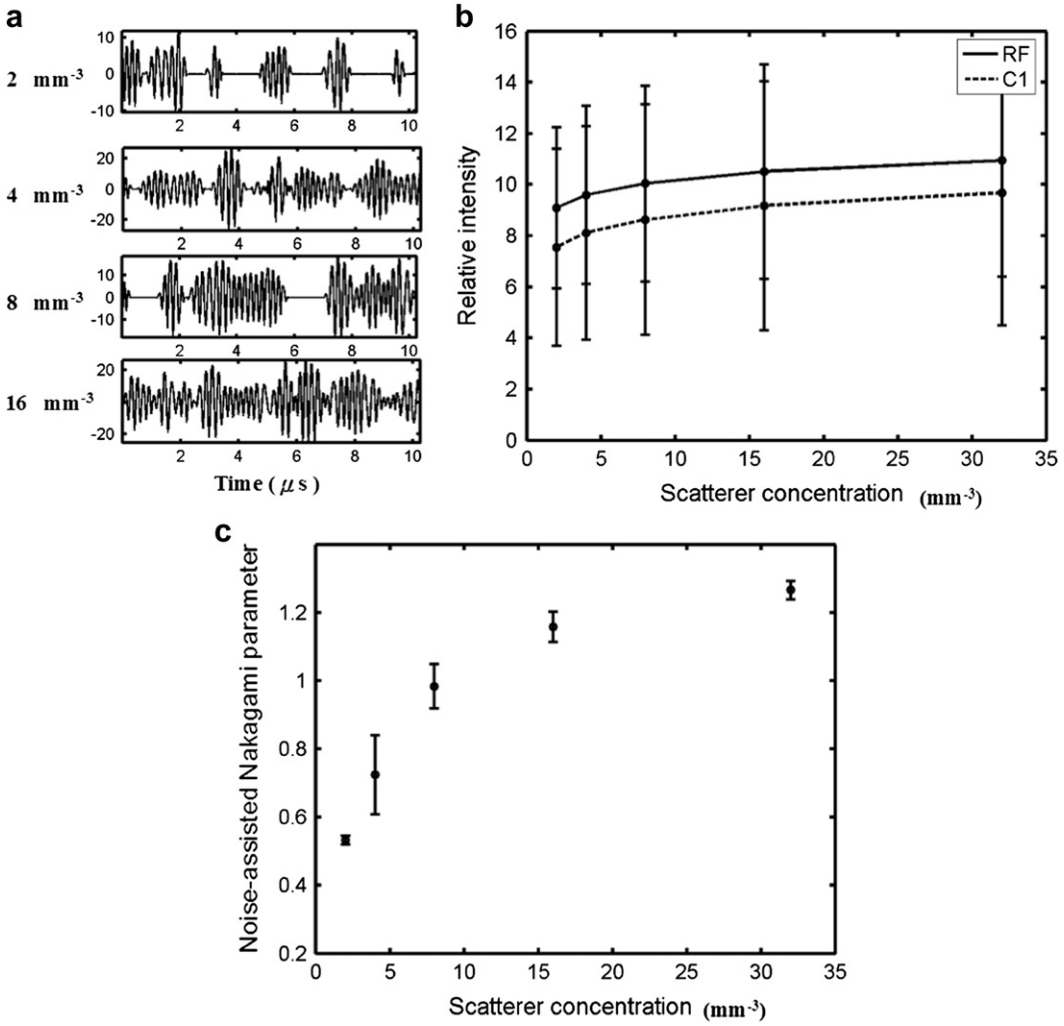

Fig. 7. (a) Filtered signals (component C1) for different scatterer concentrations from 2–16 scatterers/mm^3 (from top to bottom); (b) the relative echo intensity as a function of scatterer concentration for backscattered RF data and the C1 signal; and (c) the noise-assisted Nakagami parameter as a function of scatterer concentration. The SNR for adaptive threshold filtering was 30 dB.

a larger effect on the RF signals than when the SNR was 40 dB). Figure 7b and 7c show the relative echo intensity and the noise-assisted Nakagami parameter as functions of scatterer concentration, respectively. Comparing Figs. 6a and 7a indicates that decreasing the SNR just showed larger backscattered echoes in the output of adaptive threshold filtering (C1 signal), and the parts of signal corresponding to smaller echoes were replaced by a noise-scale baseline. In this condition, the echo intensity corresponding to each scatterer concentration for the C1 signal accordingly decreased compared with that for the RF data, as shown in Fig. 7b. Meanwhile, the noise-assisted Nakagami parameter increased from 0.5–1.2, as shown in Fig. 7c, indicating that the statistics of the backscattered signal after adaptive threshold filtering changes from a pre-Rayleigh to approximately a Rayleigh distribution as the scatterer concentration increases. This finding implies that using the adaptive threshold filter to reject smaller echoes results in the statistics of the backscattered signal measured by a nonfocused transducer varying with the scatterer concentration.

To confirm this finding, we further adjusted the SNR to 25 dB for stronger adaptive threshold filtering; the results are shown in Fig. 8. In this case, the artificial noise had a much stronger effect on the ultrasonic RF signals, and therefore it could be expected that smaller signals would be rejected by the adaptive threshold filter. Indeed, compared with the results in Fig. 7a, the C1 signals in Fig. 8a indicate the presence of significant echoes. This effect resulted in the C1 signal intensity decreasing for different scatterer concentrations, as shown in Fig. 8b. Moreover, it is interesting that the noise-assisted Nakagami parameter increased from 0.2–1 as the scatterer concentration increased from 2–32 scatterers/mm^3, as

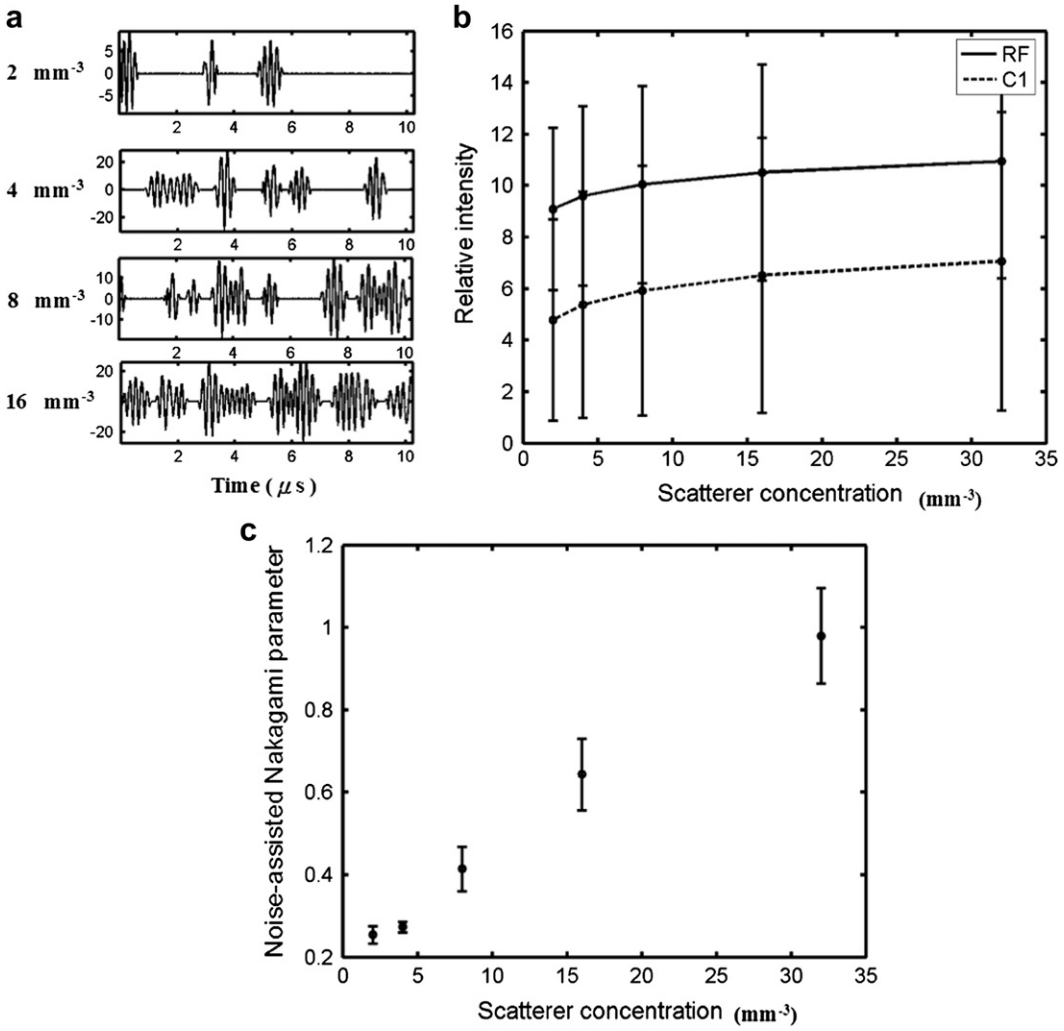

Fig. 8. (a) Filtered signals (component C1) for different scatterer concentrations from 2–16 scatterers/mm^3 (from top to bottom); (b) the relative echo intensity as a function of scatterer concentration for backscattered RF data and the C1 signal; and (c) the noise-assisted Nakagami parameter as a function of scatterer concentration. The SNR for adaptive threshold filtering was 25 dB.

shown in Fig. 8c. This result not only agrees well with that in Fig. 7c but also shows that the noise-assisted Nakagami parameter based on a nonfocused transducer is able to distinguish between different scatterer concentrations.

To explain why the noise-assisted Nakagami parameter based on a nonfocused transducer has the ability to detect variation in the scatterer concentration, consider a homogeneous medium composed of scatterers with close echogenicities, in which the backscattering intensity is typically proportional to the scatterer concentration if the effects of multiple scattering are weak. If the level of artificial noise added to the RF data is appropriate, the noise-induced fluctuations will have a larger impact on the RF signals, with smaller amplitudes for low scatterer concentrations and a lesser influence on those with larger amplitudes for high scatterer concentrations. Thus, the adaptive threshold filter will filter out more backscattered echoes for lower scatterer concentrations, causing the statistics of the backscattered signal to change from a Rayleigh to a pre-Rayleigh distribution, but it will preserve most backscattered echoes for high scatterer concentration mediums, corresponding to Rayleigh statistics.

The above theoretical explanation indicates that the noise-assisted Nakagami parameter depends on the echo intensity. However, the results from our phantom experiments indicate that the noise-assisted Nakagami parameter can still be useful. First, the adaptive threshold filter removes many low-level data in the backscattered signals. Therefore, the noise-assisted Nakagami parameter estimated using the C1 signal is likely to reflect quantitative information associated with stronger resolvable scatterers or local inhomogeneities. This is possible because there would be more locally post-Rayleigh distributed regions if the homogeneous phantom contains a higher

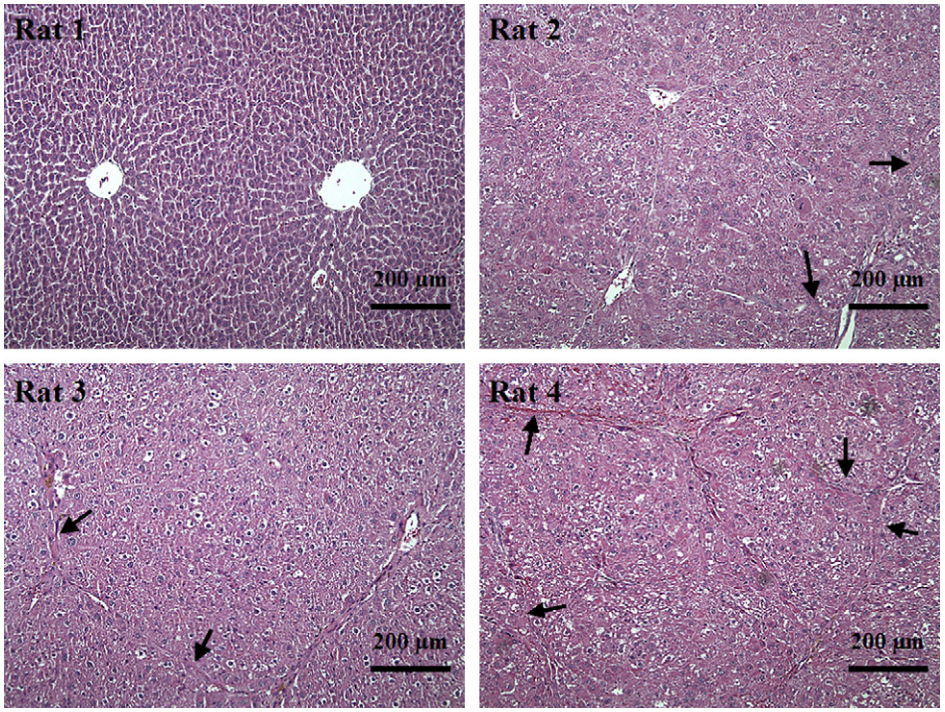

Fig. 9. H&E-stained rat liver sections of rats with different stages of liver fibrosis (100× magnification). Black arrows indicate connective fibrous tissues extending out from the portal areas.

concentration of randomly distributed scatterers (Tsui et al. 2008a). A high scatterer concentration readily results in local nonuniform spatial distributions of phantom scatterers that behave like local clusters or scatterer aggregations. This is why the noise-assisted Nakagami parameter increases with the scatterer concentration, as shown by Fig. 8c. Second, using a nonfocused transducer to measure backscattering echo intensities for the same target produces a large SD (Figs. 6b, 7b and 8b). A similar phenomenon was observed in previous studies using a nonfocused transducer to measure backscattering intensities in biological tissues (Wang and Shung 1998; Wang and Tsai 2001; Wang and Tsui 2004). However, the findings show that the measurement error is much smaller for the noise-assisted Nakagami parameter (Figs. 6c, 7c and 8c), possible reasons for which are as follows. The focal length of a nonfocused transducer used in medical imaging is determined by $D^2/4\lambda$, where D is the transducer diameter and λ is the wavelength. Therefore, the nonfocused transducer typically has a long focal length so that scatterers being imaged are in the near field of the radiation pattern where the field is not uniform and hence are subject to a strong variation in the magnitude of the axial pressure (Christensen 1988). Assuming that the scatterers have similar echogenicities, the near-field characteristics may dominantly produce a large SD in echo intensity measurements when using a nonfocused transducer. In contrast, the noise-assisted Nakagami parameter is basically determined by waveforms of the backscattered RF signals after adaptive threshold filtering, thereby reducing the dependency of the noise-assisted Nakagami parameter on the signal amplitude and the irregular radiation pattern of the near field for the nonfocused transducer.

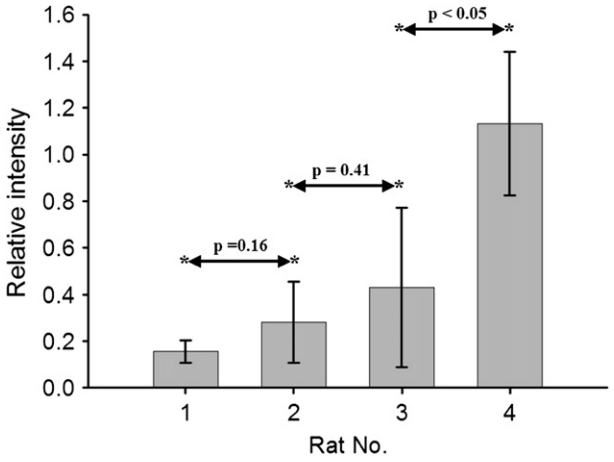

Fig. 10. Relative echo intensities for rats with different stages of liver fibrosis.

It is interesting to consider how the results might change if the backscattered data are acquired in the close part of the far field. The variation in sound pressure along the axial profile and also the beamwidth are smaller in the

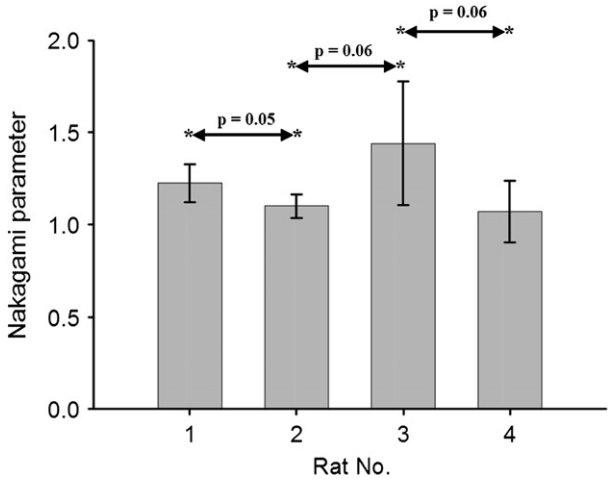

Fig. 11. Nakagami parameter for rats with different stages of liver fibrosis.

far field than in the near field. Therefore, acquiring data in the far field may reduce the SD when measuring echo intensity and therefore improve the performance of the noise-assisted Nakagami parameter in detecting variations in scatterer concentrations.

Tissue measurements

Figure 9 shows the H&E-stained rat liver sections. It was found that the amount of connective fibrous tissues (indicated by black arrows in the figure) extending out from the portal areas increased with the duration of DMN injection, demonstrating the successful induction of fibrosis. The fibrosis Metavir scores of rats 1–4, as identified by a pathologist, were normal, 0 (very weak fibrosis), 1 and 3, respectively. Figure 10 shows the results of the relative echo intensity for the excised liver specimens of different rats. The relative echo intensity increased from 0.15–1.1 as the duration of DMN injection (and hence the degree of liver fibrosis) increased. Generally speaking, the echo intensity is the most convenient index for assessing fibrosis formation (Lu et al. 1999) because the formation of fibrotic structures increases the echogenicities of scatterers in the liver (Meziri et al. 2005). However, several previous studies have indicated that the echo intensity may not be a reliable indicator and may have inadequate reproducibility in the grading and staging of liver fibrosis (Lu et al. 1999; Guimond et al. 2007). The results in Fig. 10 also agree well with those in Figs. 6b, 7b and 8b, indicating that using a nonfocused transducer to measure the echo intensity may produce a large SD such that different stages of liver fibrosis are difficult to meaningfully classify based on comparing probability values obtained from *t*-tests between rats ($p>0.05$).

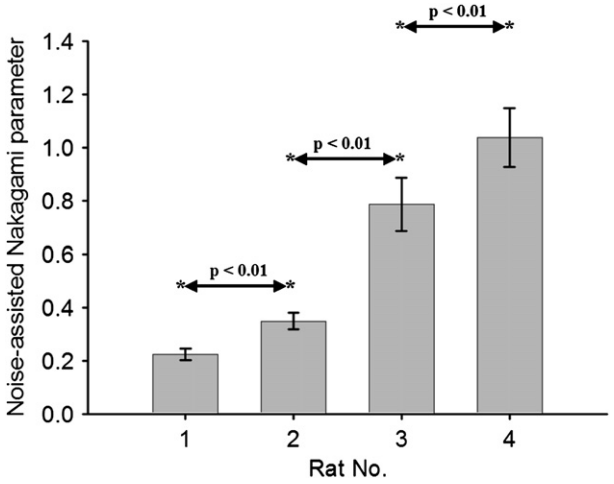

Fig. 12. Noise-assisted Nakagami parameter for rats with different stages of liver fibrosis.

Figure 11 shows the Nakagami parameter for different stages of liver fibrosis in our rats. Because we used a nonfocused transducer, the Nakagami parameter for different liver specimens was around 1, corresponding to the statistics of the backscattered envelope signals approximately conforming to a Rayleigh distribution. The probability values between each rat were also larger than 0.05, indicating that the Nakagami parameter estimated by a nonfocused transducer cannot be used to characterize scatterers in the liver.

Figure 12 shows the noise-assisted Nakagami parameter for different stages of liver fibrosis. According to the findings in phantom experiments, in this example the SNR was adjusted to 25 dB for adaptive threshold filtering. Note that the noise-assisted Nakagami parameter increased from about 0.2–1 as the fibrosis score increased, representing that the statistical distribution of the C1 component obtained by EMD of the noisy RF signals changed from a pre-Rayleigh to a Rayleigh distribution. Based on the results of our phantom experiments, the increase in the noise-assisted Nakagami parameter may represent an increase in the relative degree of local inhomogeneity due to scatterer aggregation. This is possible because fibrosis formation alters scatterer spacing and inhomogeneity in the liver (Suzuki et al. 1993; Meziri et al. 2005). Moreover, it was found that the variance of the noise-assisted Nakagami parameter was smaller within each rat liver, yielding probability values between each rat of less than 0.01. This means that classifying different stages of liver fibrosis is superior when using the noise-assisted Nakagami parameter than when using the echo intensity and the Nakagami parameter, thereby improving the performance of tissue characterization by a nonfocused transducer.

The results obtained from the phantom experiments and liver measurements have demonstrated the practical

feasibility of the method based on the noise-assisted Nakagami parameter. However, it is necessary to discuss some considerations and limitations for practical applications of the noise-assisted Nakagami parameter based on a nonfocused transducer. First, we did not apply attenuation compensation in our liver measurements. However, the results showed that the noise-assisted Nakagami parameter without attenuation correction can still be used to classify different stages of liver fibrosis in rats. This suggests that the attenuation effect does not markedly influence the use of the noise-assisted Nakagami parameter in liver characterization. Second, different systems have different types of noise effects to RF data received from the same measured target. Also, different tissues exhibit different pathological and structural changes. Thus, the SNR adjustment used for adaptive threshold filtering may need to be redetermined or corrected for different types of system and examined tissue. Third, the noise-assisted Nakagami parameter may not work when the amplitude of the intrinsic noise is comparable with or stronger than that of the measured data, since this condition reduces the quality of the received backscattered RF data, making the filter output based on component C1 of EMD a noise-based signal (Tsui et al. 2008c). Fourth, the sampling rate affects the result of EMD (Rilling and Flandrin 2006, 2009). The bandwidth of artificial noise used for adaptive threshold filtering also depends on the sampling rate, because the Nyquist theorem dictates that the maximum frequency of the artificial noise must be less than half the sampling rate. As a result, estimating the noise-assisted Nakagami parameter is dependent on the sampling rate. The present study has shown that a sampling rate of 10 times the central frequency of RF signals allows successful tissue characterization based on the noise-assisted Nakagami parameter.

CONCLUSION

This study proposes a new method for tissue characterization by a nonfocused transducer based on the noise-assisted Nakagami parameter estimated from the first IMF component (*i.e.*, component C1) obtained from EMD of noisy backscattered RF signals (*i.e.*, an adaptive threshold filtering process). To explore the feasibility of the proposed method, experiments were performed on phantoms with different scatterer concentrations and *in vitro* measurements were made on rat livers with and without induced fibrosis. From the results we can draw the following conclusions: (1) The conventional Nakagami parameter cannot be used to distinguish different scatterer properties with a nonfocused transducer; (2) the noise-assisted Nakagami parameter based on a nonfocused transducer performed well in classifying phantoms with different scatterer concentrations; (3) the measurements on rat livers at various stages of fibrosis demonstrated that the method based on the noise-assisted Nakagami parameter has feasible practicality; (4) using the noise-assisted Nakagami parameter can avoid generating a large measurement error when using a nonfocused transducer to measure the echo intensity or the conventional Nakagami parameter for characterizing tissues; and (5) the meanings of the conventional Nakagami parameter and the noise-assisted Nakagami parameter differ with the characteristics of the adaptive threshold filter. The Nakagami parameter represents the statistics of the signal backscattered from unresolvable scatterers, whereas the noise-assisted Nakagami parameter is associated with stronger resolvable scatterers or local inhomogeneities caused by scatterer aggregation that are useful for evaluating pathological stages in a tissue (*e.g.*, liver fibrosis).

Acknowledgements—This work was supported by Academia Sinica under Grant No. AS-98-TP-A02 and the National Science Council of the Republic of China (Taiwan) under Grant Nos. NSC95-2119-M-008-031-MY3 and NSC98-2627-B-008-004. The authors would like to acknowledge the reviewers for their valuable comments.

REFERENCES

Bevan PD, Sherar MD. B-scan ultrasound imaging of thermal coagulation in bovine liver: Frequency shift attenuation mapping. Ultrasound Med. Biol. 2001;27:809–817.

Boashash B. Estimating and interpreting the instantaneous frequency of a signal—Part 1: Fundamentals. Proc IEEE 1992;80:520–538.

Burckhardt CB. Speckle in ultrasound B-mode scans. IEEE Trans Sonics Ultrason 1978;SU-25:1–6.

Christensen DA. Ultrasonic bioinstrumentation. New York: Wiley; 1988.

Cloutier G, Daronatand M, Savery D, Garcia D, Durand LG, Foster FS. Non-Gaussian statistics and temporal variations of the ultrasound signal backscattered by blood at frequencies between 10 and 58 MHz. J Acoust Soc Am 2004;116:566–577.

Dutt V, Greenleaf JF. Ultrasound echo envelope analysis using a homodyned K distribution signal model. Ultrason Imag 1994;16:265–287.

Dumane VA, Shankar PM. Use of frequency diversity and Nakagami statistics in ultrasonic tissue characterization. IEEE Trans Ultrason Ferroelectr Freq Control 2001;48:1139–1146.

Flandrin P, Rilling G, Goncalves P. Empirical mode decomposition as a filter bank. IEEE Signal Proc Lett 2004;11:112–114.

George J, Rao KR, Stenr R, Chandrakasan G. Dimethylnitrosamine-induced liver injury in rats: The early deposition of collagen. Toxicology 2001;156:129–138.

Guimond A, Teletin M, Garo E, D'Sa A, Selloum M, Champy MF, Vonesch JL, Monassier L. Quantitative ultrasonic tissue characterization as a new tool for continuous monitoring of chronic liver remodelling in mice. Liver Int 2007;27:854–864.

Hampshire JBI, Strohbehn JW, McDaniel MD, Waugh JL, James DH. Probability density of myocardial ultrasonic backscatter. Proceedings of the 14th Annual Northeast Bioengineering Conference 1988;March:305–308.

Huang CC, Wang SH. Statistical variations of ultrasound signals backscattered from flowing blood. Ultrasound Med Biol 2007;33:1943–1954.

Huang NE, Shen Z, Long SR, Wu MC, Shih HH, Zheng Q, Yen NC, Tung CC, Liu HH. The empirical mode decomposition method and the Hilbert spectrum for nonlinear and non-stationary time series analysis. Proc Royal Soc London A 1998;454:903–995.

Huang NE, Shen Z, Long SR. A new view of nonlinear water waves: The Hilbert spectrum. Annu Rev Fluid Mech 1999;31:417–457.

Karmeshu, Agrawal R. Study of ultrasonic echo envelope based on Nakagami-inverse Gaussian distribution. Ultrasound Med Biol 2006;32:371–376.

Lu ZF, Zagzebski JA, Lee FT. Ultrasound backscatter and attenuation in human liver with diffuse disease. Ultrasound Med Biol 1999;25: 1047–1054.

Meziri M, Pereirab WCA, Abdelwahabc A, Degottd C, Laugierc P. In vitro chronic hepatic disease characterization with a multiparametric ultrasonic approach. Ultrasonics 2005;43:305–313.

Nadarajah S. Statistical distributions of potential interest in ultrasound speckle analysis. Phys Med Biol 2007;52:N213–N227.

Oosterveld BJ, Thijssen JM, Verhoef WA. Texture of B-mode echograms: 3-D simulations and experiments of the effects of diffraction and scatter density. Ultrason Imag 1985;7:142–160.

Raju BI, Srinivasan MA. Statistics of envelope of high-frequency ultrasonic backscatter from human skin in vivo. IEEE Trans Ultrason Ferroelectr Freq Control 2002;49:871–882.

Rilling G, Flandrin P. On the influence of sampling on the empirical mode decomposition. ICASSP 2006;3:444–447.

Rilling G, Flandrin P. Sampling effects on the empirical mode decomposition. Adv Adaptive Data Anal 2009;1:43–59.

Schwartz M, Bennett WR, Stein S. Communications systems and techniques. New York: McGraw-Hill; 1966.

Shankar PM. A model for ultrasonic scattering from tissues based on K-distribution. Phys Med Biol 1995;40:1633–1649.

Shankar PM. A general statistical model for ultrasonic backscattering from tissues. IEEE Trans Ultrason Ferroelectr Freq Control 2000; 47:727–736.

Shankar PM, Dumane VA, Reid JM, Genis V, Forsberg F, Piccoli CW, Goldberg BB. Classification of ultrasonic B-mode images of breast masses using Nakagami distribution. IEEE Trans Ultrason Ferroelectr Freq Control 2001;48:569–580.

Shankar PM, Dumane VA, George T, Piccoli CW, Reid JM, Forsberg F, Goldberg BB. Classification of breast masses in ultrasonic B scans using Nakagami and K distributions. Phys Med Biol 2003;48:2229–2240.

Shankar PM. A compounding scattering pdf for the ultrasonic echo envelope and its relationship to K and Nakagami distributions. IEEE Trans Ultrason Ferroelectr Freq Control 2003;50:339–343.

Shankar PM. The use of the compounding probability density function in ultrasonic tissue characterization. Phys Med Biol 2004;49:1007–1015.

Shung KK, Thieme GA. Ultrasonic scattering in biological tissues. Boca Raton: CRC Press; 1993.

Suzuki K, Hayashi N, Sasaki Y, Kono M, Kasahara A, Imai Y, Fusamoto H, Kamada T. Evaluation of structural change in diffuse liver disease with frequency domain analysis of ultrasound. Hepatology 1993;17:1041–1046.

Tsui PH, Wang SH. The effect of transducer characteristics on the estimation of Nakagami parameter as a function of scatterer concentration. Ultrasound Med Biol 2004;30:1345–1353.

Tsui PH, Chang CC. Imaging local scatterer concentrations by the Nakagami statistical model. Ultrasound Med. Biol 2007;33:608–619.

Tsui PH, Huang CC, Chang CC, Wang SH, Shung KK. Feasibility study of using high-frequency ultrasonic Nakagami imaging for characterizing the cataract lens in vitro. Phys Med Biol 2007;52:6413–6425.

Tsui PH, Yeh CK, Chang CC, Chen WS. Performance evaluation of ultrasonic Nakagami image in tissue characterization. Ultrason Imag 2008a;30:78–94.

Tsui PH, Yeh CK, Chang CC, Liao YY. Classification of breast masses by ultrasonic Nakagami imaging: A feasibility study. Phys Med Biol 2008b;53:6027–6044.

Tsui PH, Chang CC, Chang CC, Huang NE, Ho MC. An adaptive threshold filter for ultrasound signal rejection. Ultrasonics 2008c; 49:413–418.

Tuthill TA, Sperry RH, Parker KJ. Deviations from Rayleigh statistics in ultrasonic speckle. Ultrason Imag 1988;10:81–89.

Wachowiak MP, Smolikova R, Tourassi GD, Elmaghraby AS. General ultrasound speckle models in determining scatterer density. Proc SPIE 2002;4687:285–295.

Wagner RF, Insana MF, Brown DG. Statistical properties of radiofrequency and envelope detected signals with applications to medical ultrasound. J Opt Soc Am 1987;4:910–922.

Wang CY, Shung KK. Variation in ultrasonic backscattering from skeletal muscle during passive stretching. IEEE Trans Ultrason Ferroelectr Freq Control 1998;45:504–510.

Wang SH, Shung KK. An approach for measuring ultrasonic backscattering from biological tissues with focused transducers. IEEE Trans Biomed Eng 1997;44:549–554.

Wang SH, Tsai FC. Characterization of bony tissues from ultrasonic backscattering using statistical models. IEEE Ultrason Symp Proc 2001;2:1205–1208.

Wang SH, Tsui PH. Ultrasonic techniques to assess the properties of hard and soft biological tissues. Key Eng Material 2004;270-273: 2055–2060.

Weng L, Reid JM, Shankar PM, Soetanto K. Ultrasound speckle analysis based on the K distribution. J Acoust Soc Am 1991;89:2992–2995.

Yuan YW, Shung KK. The effect of focusing on ultrasonic backscatter measurements. Ultrason Imag 1986;8:121–130.

Zagzebski JA, Chen JF, Dong F, Wilson T. Intervening attenuation affects first-order statistical properties of ultrasound echo signals. IEEE Trans Ultrason Ferroelectr Freq Control 1999;46:35–40.

Zimmer Y, Akselrod S, Tepper R. The distribution of the local entropy in ultrasound images. Ultrasound Med Biol 1996;22:431–439.